Electronic Supplementary Material (ESI) for Nanoscale.

Supporting materials to: Transport of nanoprobes in multicellular spheroids

Marta Pilz [a], Karina Kwapiszewska [a,*], Tomasz Kalwarczyk [a], Grzegorz Bubak [a], Dominika Nowis [b,c], and Robert Hołyst [a,*]

[a] Department of Soft Condensed Matter, Institute of Physical Chemistry, Polish Academy of Sciences, Warsaw, Poland

[b] Genomic Medicine, Medical University, Warsaw, Poland

[c] Laboratory of Experimental Medicine, Centre of New Technologies, University of Warsaw, Poland

*** Corresponding authors, e-mail: kkwapiszewska@ichf.edu.pl, rholyst@ichf.edu.pl**

Culture of spheroids

Daily monitoring of spheroid formation and growth was done using the phase contrast mode of Nikon Eclipse Ti-S Inverted Microscope. Below, on Figures S1-S3 we show images of spheroids of three different human cell lines used in our research. The presented spheroids are suspended in the proper growth medium and have been growing in the Nunclon™ Sphera™ dishes. Each image was captured on the 4th day of spheroids culture.

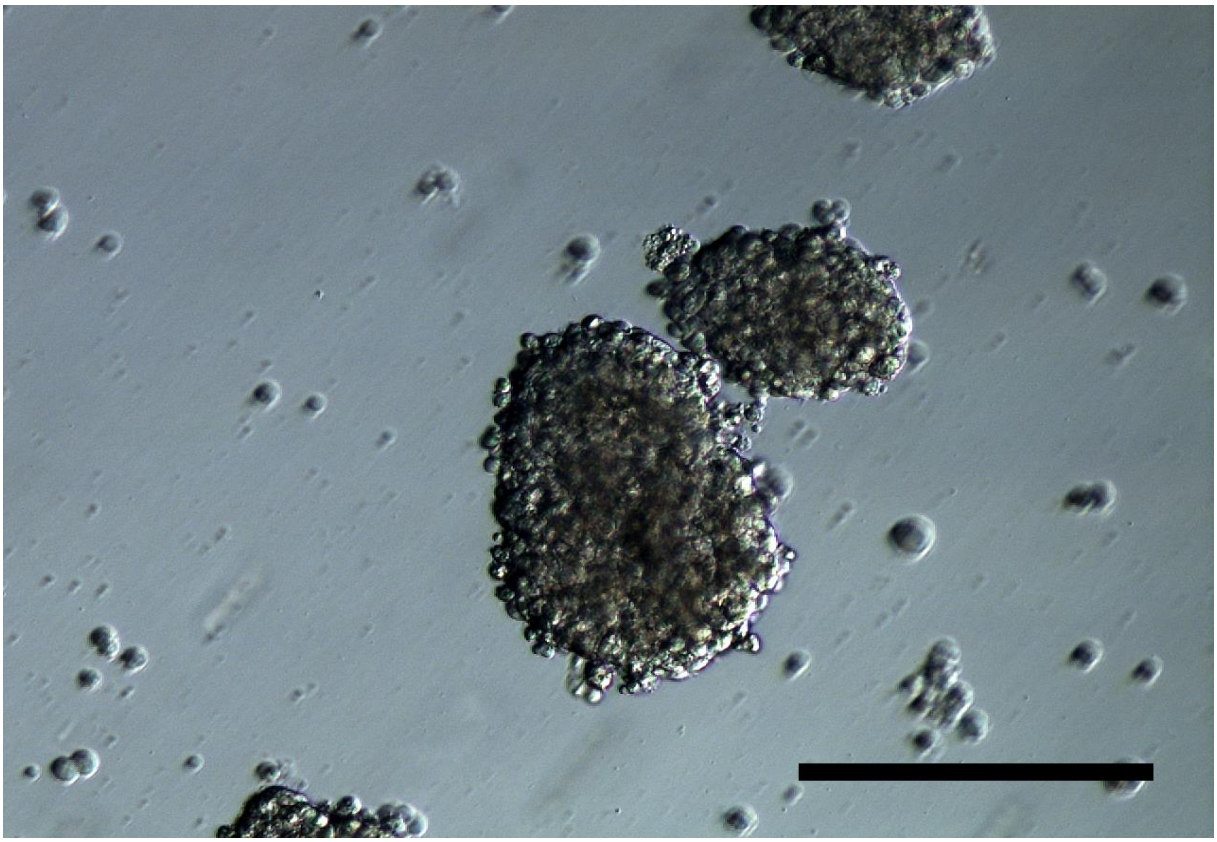

Figure S1. The spheroids of HeLa cells. Scale bar corresponds to 250 μm.

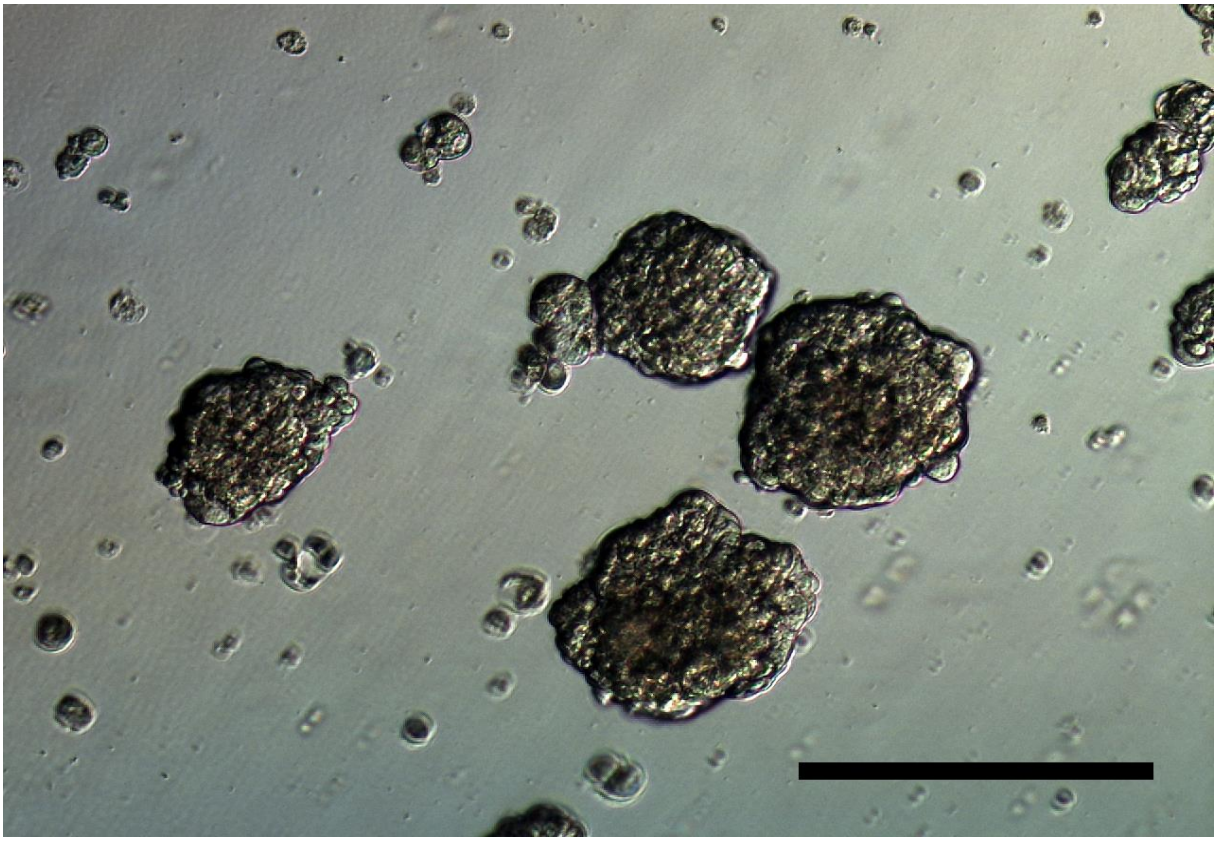

Figure S2. The spheroids of MCF-7 cells. Scale bar corresponds to 250 μm.

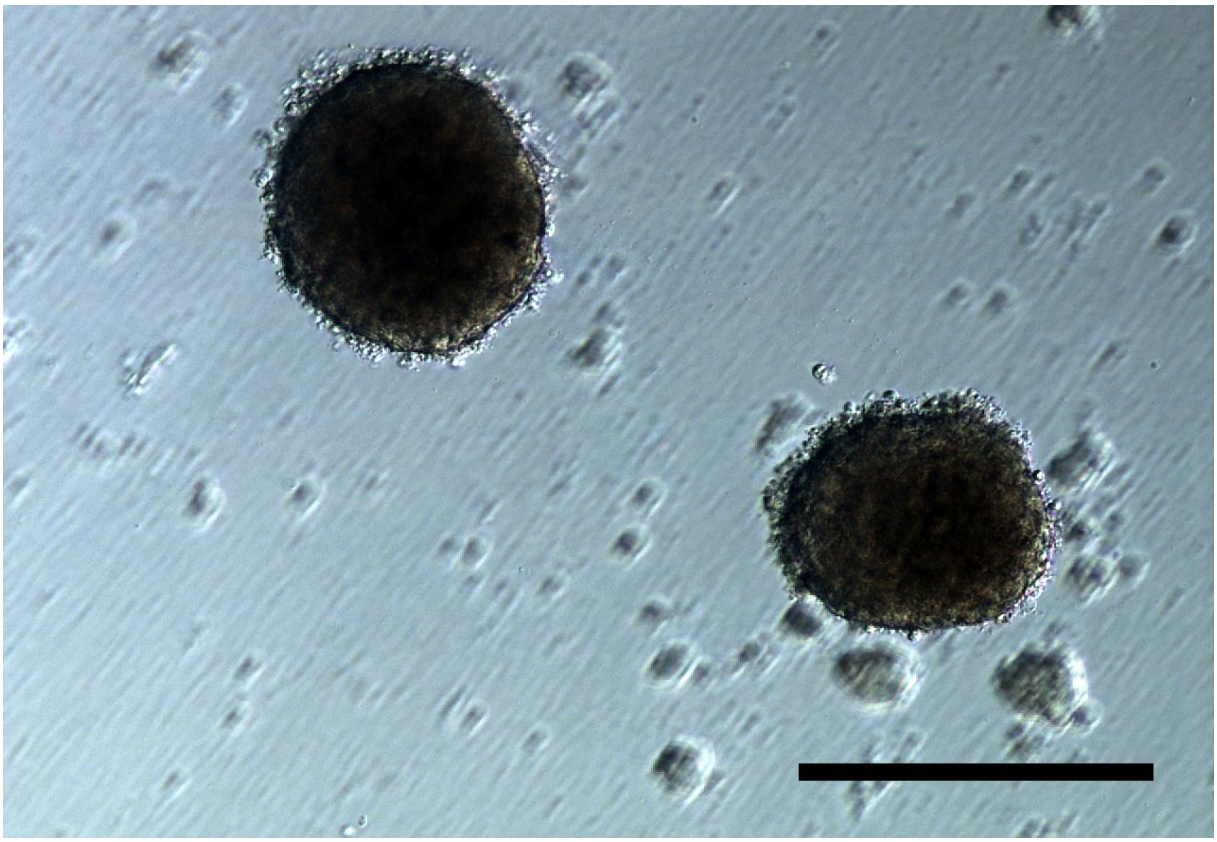

Figure S3. The spheroids of fibroblast cells. Scale bar corresponds to 250 μm.

Z-stack images of spheroids

At the fifth day of spheroid cultivation, spheroids were stained with 2 μM calcein-AM (ThermoFisher, USA) to visualise their 3D structure. The samples were incubated with dye for 3 h before imaging. Then, images were taken using Z-scanning mode of the confocal microscope Nikon A1 with FITC channels.

However, one has to remember that below images demonstrate the shape of spheroids as well as the limitations of confocal imaging for capturing the full 3D geometry of spheroids.

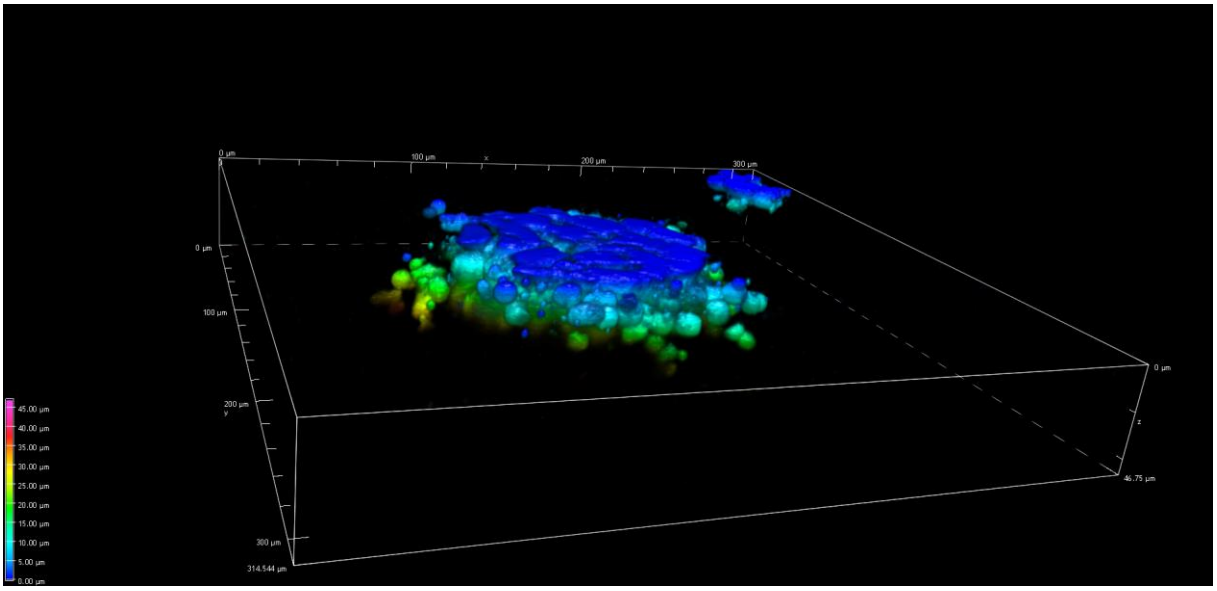

Figure S4. Z-stack confocal image of HeLa spheroid stained with calcein-AM. The colour represents the z-depth as indicated by the depth scale on the image (blue is indicative of minimum depth, while red is the maximum depth of around 50 μm).

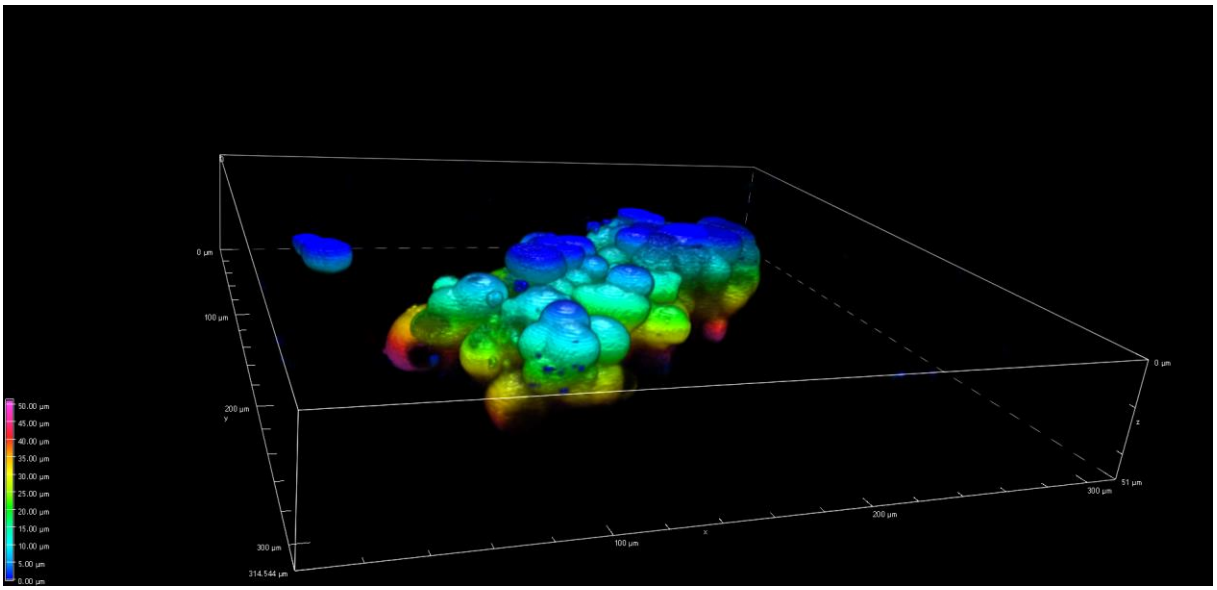

Figure S5. Z-stack confocal image of MCF-7 spheroid stained with calcein-AM. The colour represents the z-depth as indicated by the depth scale on the image (blue is indicative of minimum depth, while red is the maximum depth of around 50 μm).

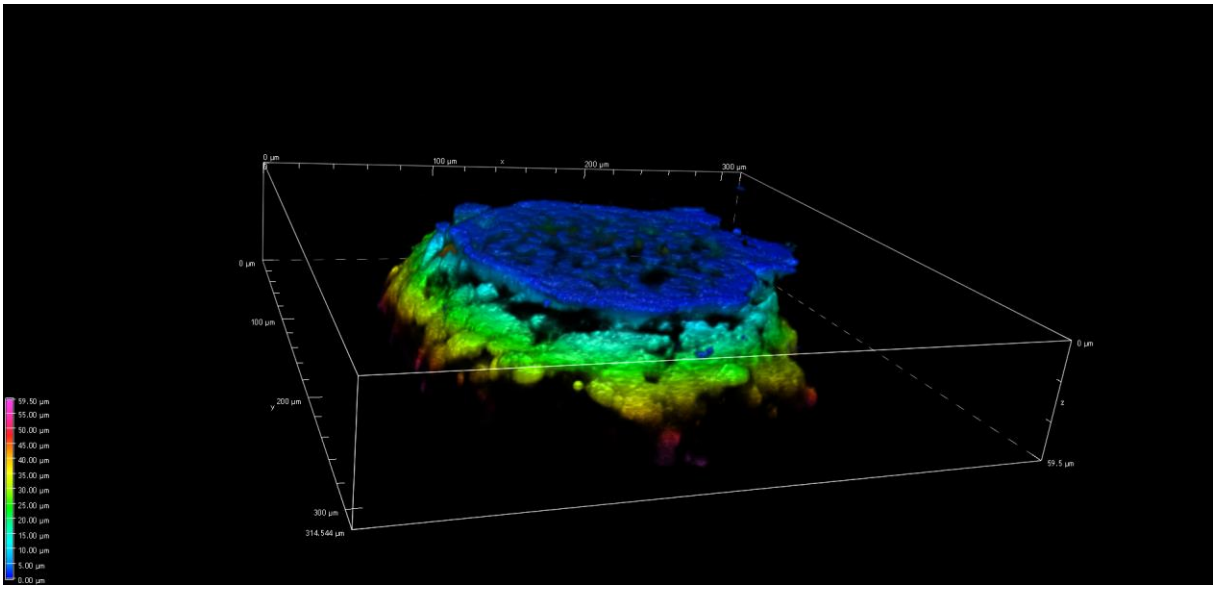

Figure S6. Z-stack confocal image of fibroblasts spheroid stained with calcein-AM. The colour represents the z-depth as indicated by the depth scale on the image (blue is indicative of minimum depth, while red is the maximum depth of around 50 µm).

The positioning of the detection volume within the ECM of spheroids

The focal volume was precisely positioned in the extracellular area by using the imaging mode of the Nikon C1 microscope. Below (Figure S7), we present the exemplary image of the spheroid's cross-section to visualise the procedure of positioning. First, it was crucial to exclude cellular space. The cellular autofluorescence (excited by 485 nm laser) enabled the easy localisation of the cells and revealed their edges. The blue laser was used only for positioning of cells and after that was immediately switched off. Simultaneous 561 nm laser excitation of tracers indicated the localisation of the extracellular space. So defined the extracellular and cellular regions of spheroids allowed for the further adjustment of the three axis.

The Z plane was established at a maximum depth of 30 μm inside the spheroids. This limited depth arises from light scattering by further layers of cells within spheroids. Then, by moving the X-Y stage, we selected the position of detection volume at the distance of 2-10 μm from the cell edges. The accuracy of alignment was within 1 µm. Once determined, the position is marked in the imaging mode, and after a switch to the FCS mode, the records were taken.

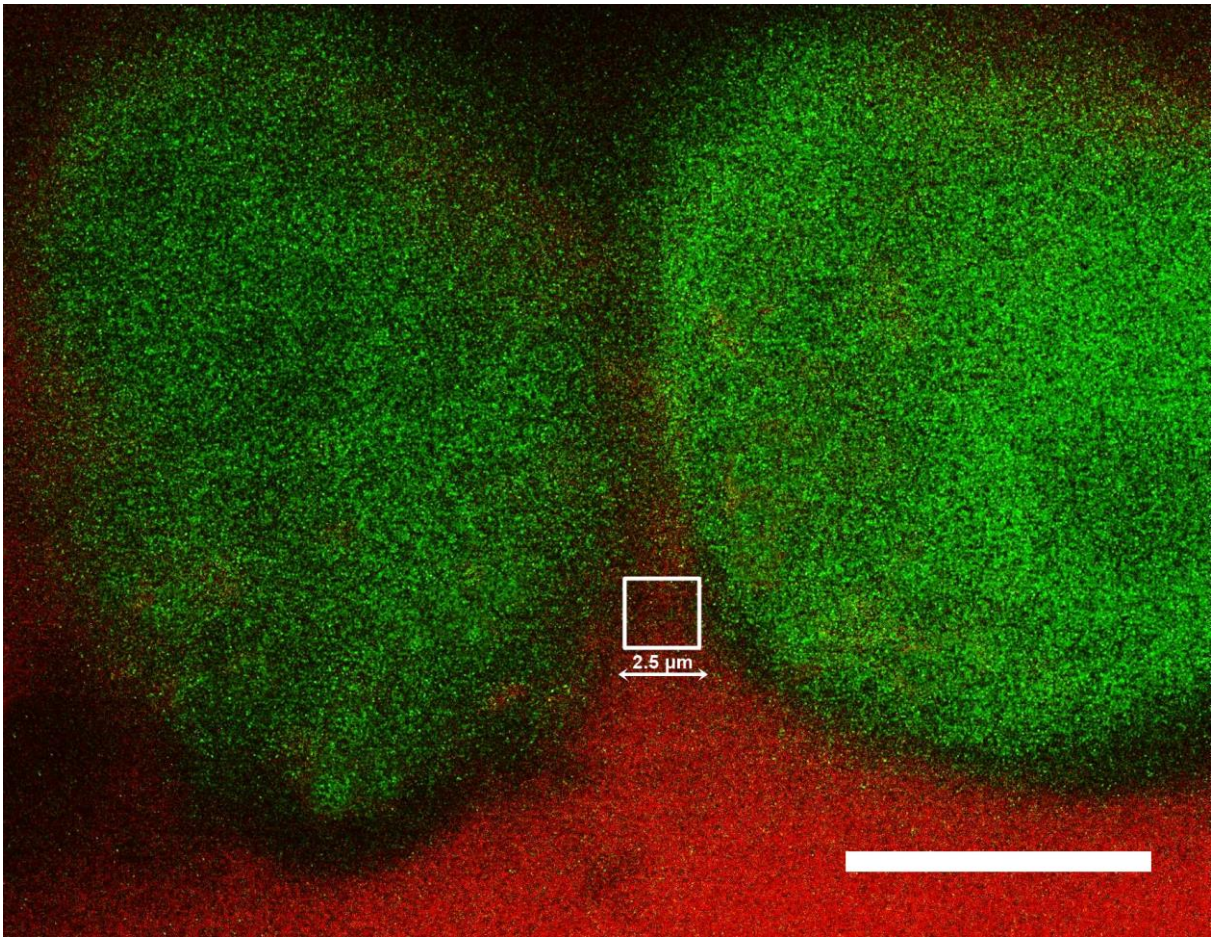

Figure S7. The positioning of the confocal volume within the ECM of spheroids at 30 μm depth. For the clear imaging purpose only, we used HeLa-EGFP cell line [1]. The green fluorescence signal originates from EGFP expressed by HeLa cells, while the red ones respond to the dextran 155 kDa molecules in the extracellular matrix. The white box depicts an exemplary region of the ECM chosen for FCS measurements. The focal volume was placed far from the cellular membrane. Therefore the molecules which are inside the cells do not alter the FCS measurements in the ECM. If the extracellular spaces with bright spots were present (corresponding to aggregates of molecules), we avoided them in the experiments. The scale bar is 10 μm.

Fluorescent imaging of the ECM – control

In prior to visualising the ECM structure within spheroids, the negative control was performed using cell cultured as a monolayer. HeLa cells were seed on the CELLview™ (Greiner Bio-One, Austria) dish. When the cell attached to the surface, Col-F was added to a final concentration of 10 μM in a cell culture medium. After 1 h incubation at 37℃, cells were washed 3 times with PBS and imaged. Based on Figure S8 we excluded binding Col-F to the cell membrane and its penetration to the cell interior.

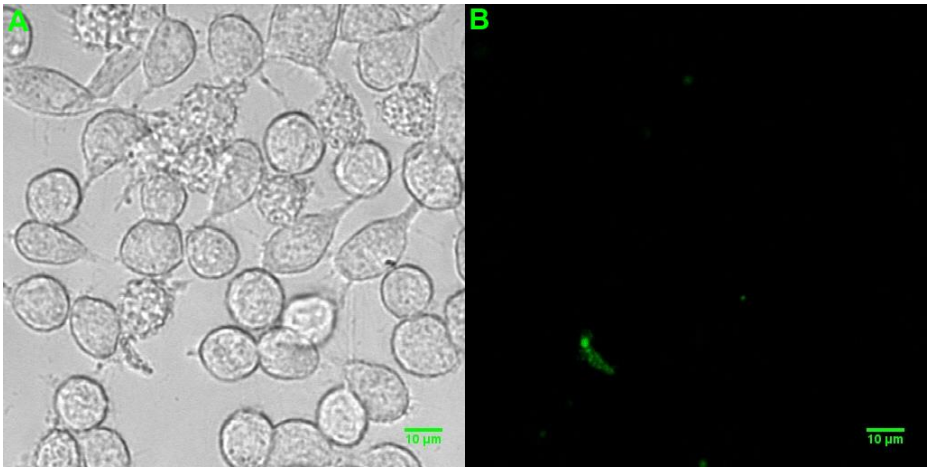

Figure S8. A. The optical transmission image of HeLa monolayer culture after 1h incubation with Col-F. Panel B depicts that this fluorescent dye does not penetrate the cell interior as well as monolayer cell culture do not secrete elastic and collagenous fibres. The object stained with Col-F is cell debris.

Experimental data

FCS data obtained for dextrans were fitted using the model of single component anomalous diffusion [2] In this case, the autocorrelation function $G(t)$ is in the form:

$$G(t) = \left(1 + \frac{T}{1-T} \cdot e^{-t/\tau_T}\right)\left(\frac{1}{N}\right)\frac{1}{\left(1 + \left(\frac{t}{\tau_{D_t}}\right)^{\alpha}\right)\left(1 + \frac{1}{\kappa^2}\left(\frac{t}{\tau_{D_t}}\right)^{\alpha}\right)^{1/2}} \quad \text{(S1)}$$

where: T is the fraction of dye molecules in triplet state and τ_T is the triplet lifetime, N stands for the average number of fluorescent probes inside the focal volume, τ_{D_t} is the time of translational diffusion, α is the anomality index, and κ is the aspect ratio of the focal volume (measured during calibration).

Figure S9 shows the experimental data, including 5 autocorrelation curves plotted together (red curves). The mean diffusion time for the tracer was obtained from the fit of the averaged autocorrelation of the 5 correlation curves (plotted as a purple curve).

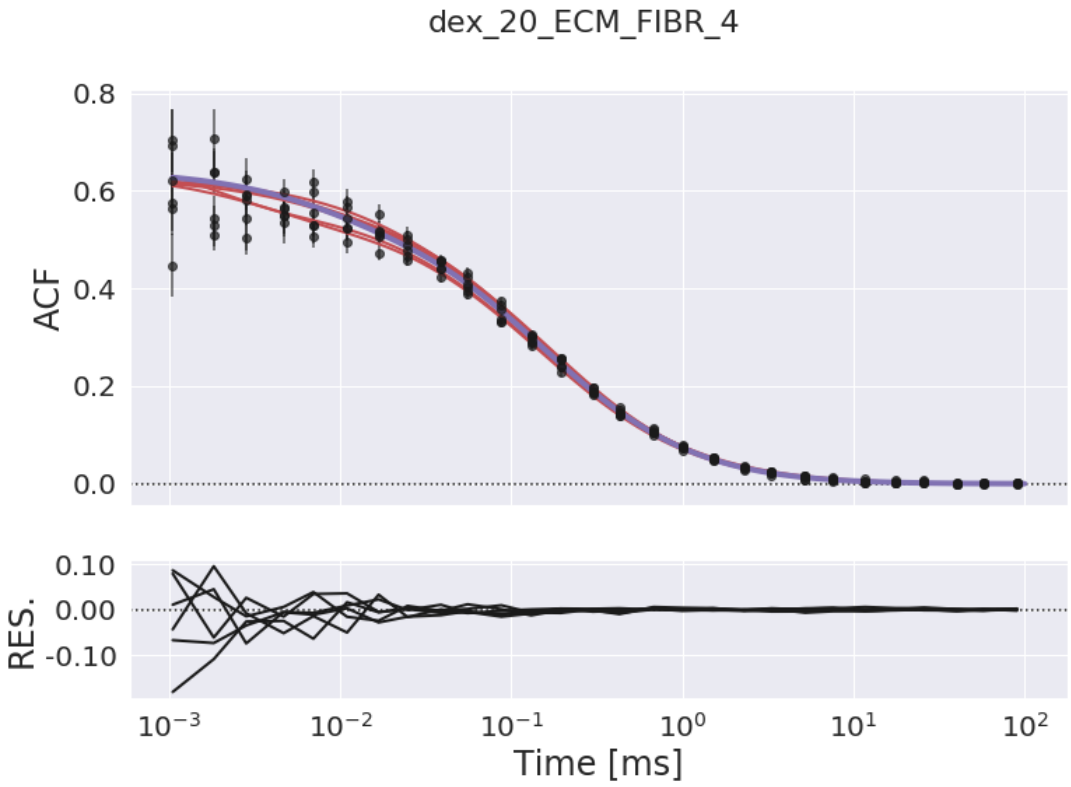

Figure S9. Example of the FCS autocorrelation curves for dextran 20 kDa in ECM of the fibroblast spheroid (black points, every 10th point plotted). Measuring time for each autocorrelation curve was 25 s. The data were fitted with the anomalous diffusion model, including the triplet state contribution (Equation S1). The bottom panel shows the residual curve.

In the case of nanoparticles' diffusion, we applied the autocorrelation function $G(t)$ describing single component anomalous diffusion, also taking into account the rotational mode (first term of the Equation S2):

$$G(t) = \left(1 + \left[A_1 \exp\left(-\frac{t}{t_{D_r}}\right)\right] + \left[A_2 exp\left(-\frac{10t}{3t_{D_r}}\right)\right]\right) \times \left(\frac{1}{N}\right) \frac{1}{\left(1 + \left(\frac{t}{\tau_{D_t}}\right)^{\alpha}\right)\left(1 + \frac{1}{\kappa^2}\left(\frac{t}{\tau_{D_t}}\right)^{\alpha}\right)^{1/2}} \quad \text{(S2)}$$

where: A_1 and A_2 stand for the amplitudes of rotational mode and t_{D_r} is the time of rotational diffusion.

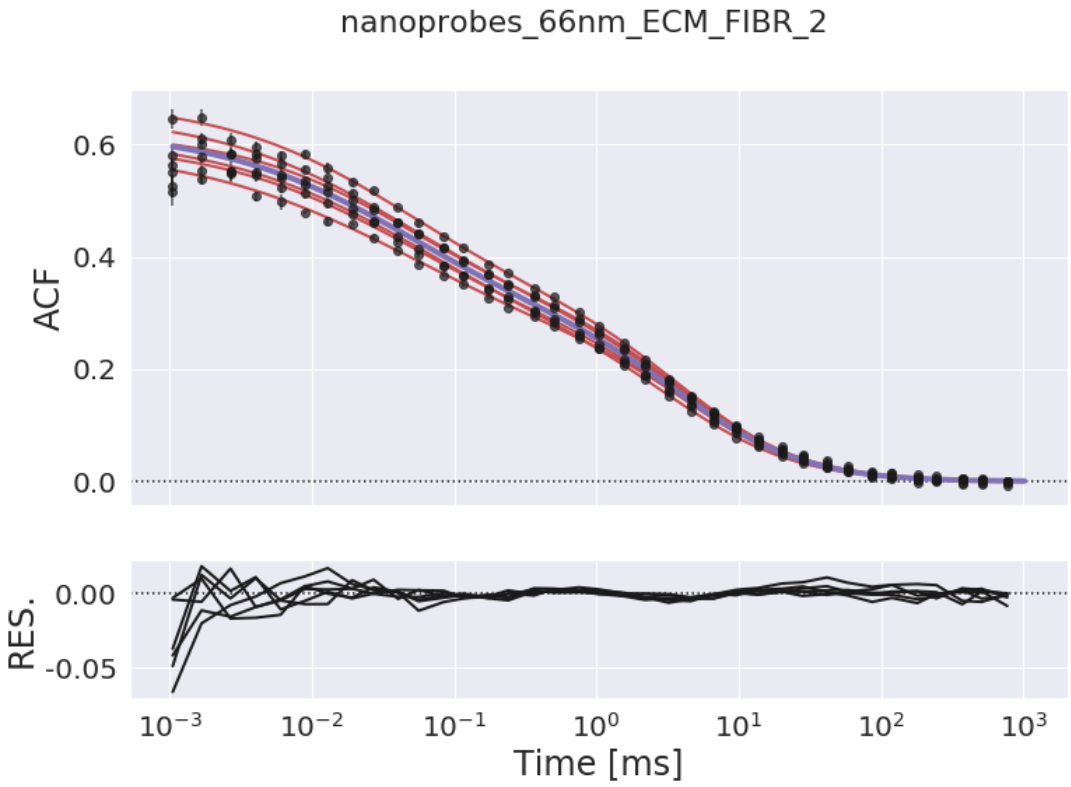

Figure S10. Example of the FCS autocorrelation curve for nanoparticles S43(2) in ECM of the fibroblast spheroid (black points, every 10th point plotted). Measuring time for each autocorrelation curve was 120 s. The data were fitted with the model described by Equation S2. The bottom panel shows the residual curve. Changes in the amplitudes for each measurement do not follow systematic decrease – no photobleaching was observed, only change in a number of nanoparticles due to diffusion.

Influence of physical properties of nanoparticles on their movement in viscous fluids

The main competing forces acting on the motion of an individual uncharged particle in the viscous fluid are gravity, buoyancy and hydrodynamic drag. For a spherical particle, sedimentation force (gravity and buoyancy) are given by:

$$\overrightarrow{F_g} = \frac{4}{3}\pi R^3(\rho_p - \rho_f)\vec{g}$$

where ρ_p is the density of the particle, ρ_f is the density of the fluid, R is the particle radius, and g is the acceleration of gravity.

The hydrodynamic drag (for small Reynolds numbers) on a spherical particle is given by:

$$\overrightarrow{F_d} = 6\pi\eta R\vec{v}$$

Where η is the viscosity of the fluid, $\vec{v}$ is particle velocity.

A force-balance of gravity, buoyancy and hydrodynamic drag yields the sedimentation velocity of a single particle sedimenting in the fluid of viscosity η as:

$$v = \frac{2R^2(\rho_p - \rho_f)g}{9\,\eta}$$

The sedimentation speed depends on physical properties of particles – its size and density. In addition to motion related with settling of particles, the stochastic motion occurs and is characterised by a self-diffusion coefficient, which does not depend on the density and is the same for any (i.e. carbon, silica or gold) same-sized nanoparticles:

$$D = \frac{kT}{6\pi\eta R}$$

Where k is the Boltzmann constant, $T(K)$ is temperature. The diffusion coefficient is defined through the mean square displacement:

$$\langle x^2 \rangle = 6Dt$$

To estimate how the density of particles affects the calculation of effective viscosity, we consider which effect dominates - the molecular displacement due to the sedimentation of particle or due to the Brownian motion?

The missing parameter to estimate the exact value of sedimentation velocity is the density of the fluid ρ_f – in our case the density of the extracellular matrix. Here, we assume the density of water, $\rho_f = 997\ kg/m^3$, the actual (for sure greater) density value will increase the sedimentation velocity, since $v \propto \Delta\rho$.

If we consider **silica nanoparticles** ($\rho_p = 2650\ kg/m^3$) with radius R =111 nm (the biggest nanoprobe used in experiments) moving in the ECM of HeLa cells which viscosity we found to be $\eta_{macro} = 3.32\ mPa \cdot s$, the sedimentation speed is approximately 13 nm/s. Therefore, during the 120 seconds (the time of data acquisition) particle will cross a distance L =1.6 μm ($L = vt$). While the root mean displacement x of the same nanoprobe resulting from Brownian motion (the determined from experiment diffusion coefficient equals to D=0.66 $\mu m^2/s$) is around 22 μm. We can clearly see that $x \gg L$.

Since **carbon nanoparticles** have similar density ($\rho_p = 2260\ kg/m^3$) as silica nanoparticles, the sedimentation is also negligible.

In the case of **gold nanoparticles** ($\rho_p = 19320\ kg/m^3$) with the same radius, moving in the same environment, the sedimentation velocity is 148 nm/s. After a time, $t = 120\ s$ the molecular displacement resulting from settling equals 18 μm – it is comparable distance with the root mean displacement resulting from diffusion, $L \sim x$.

To conclude, the physical properties of nanoparticles, such as density may contribute to their transport properties. However, in the case of silica nanoparticles used in our experiments, the diffusion was a prevailing process, and in consequence, the calculation of effective viscosity was done correctly.

Heterogeneity of the ECM

Following the approach of Stiehl and Weiss [3] for tracking the heterogeneity of the medium, we performed measurements of diffusivity for S34(1) nanoparticles within the ECM of HeLa spheroids (Figure S11). We found large deviations in the diffusion time of nanoparticles. The diffusion times of analysed probes were changing from 1 ms up to 4 ms. The short diffusion times suggest the presence of large free extracellular spaces. On the contrary slow-moving probes (long diffusion times) probe fibrous-rich areas. However, if there were only fibrous-rich and fibrous-free areas, the bimodal distribution would be obtained. In our case, the distribution is wide and quite uniform, what points at the heterogeneity of the ECM structure - the presence of the different matrix pore sizes, an intrinsic disorder of the fibre network, and uneven distribution of the ECM components. The heterogeneity of the ECM structure was additionally illustrated in Figure S12.

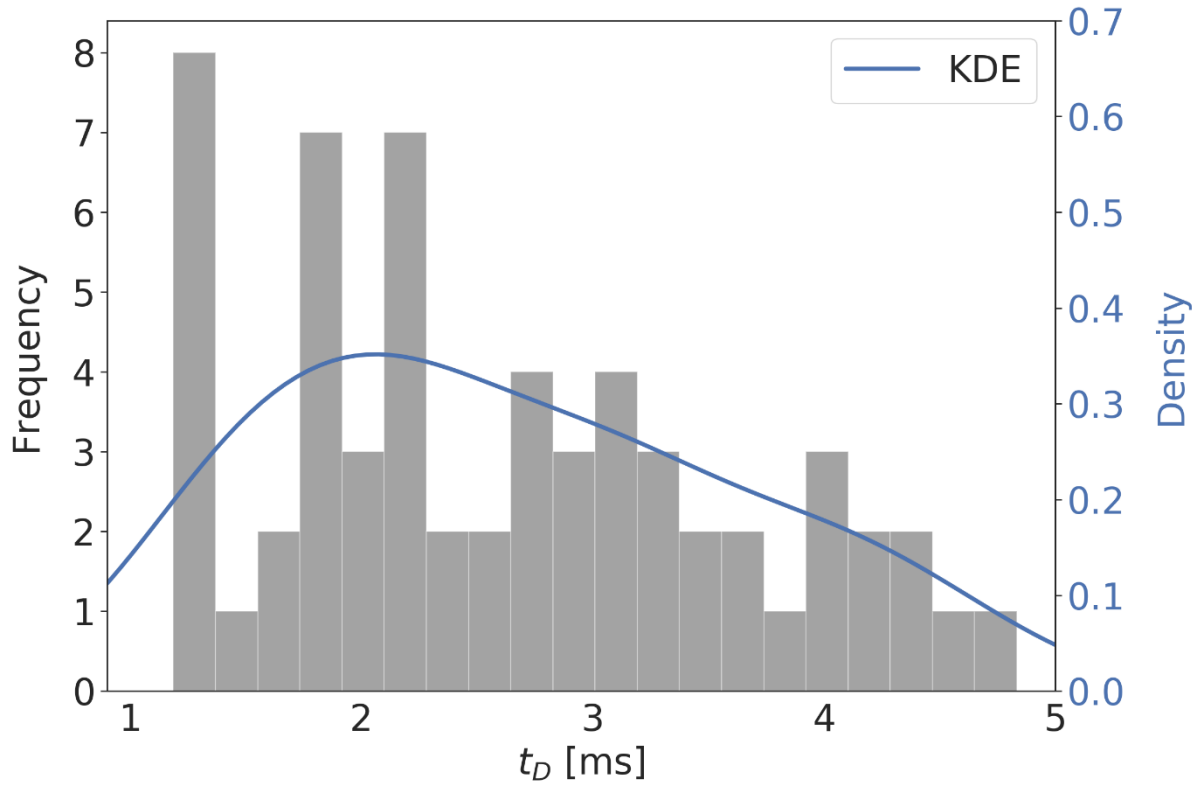

Figure S11. Histogram showing the distribution ($N = 60$) of a measured diffusion time for nanoparticle S34(1) within the ECM of HeLa spheroids. The solid blue line corresponds to kernel density estimation (KDE) of the histogram (right y-axis).

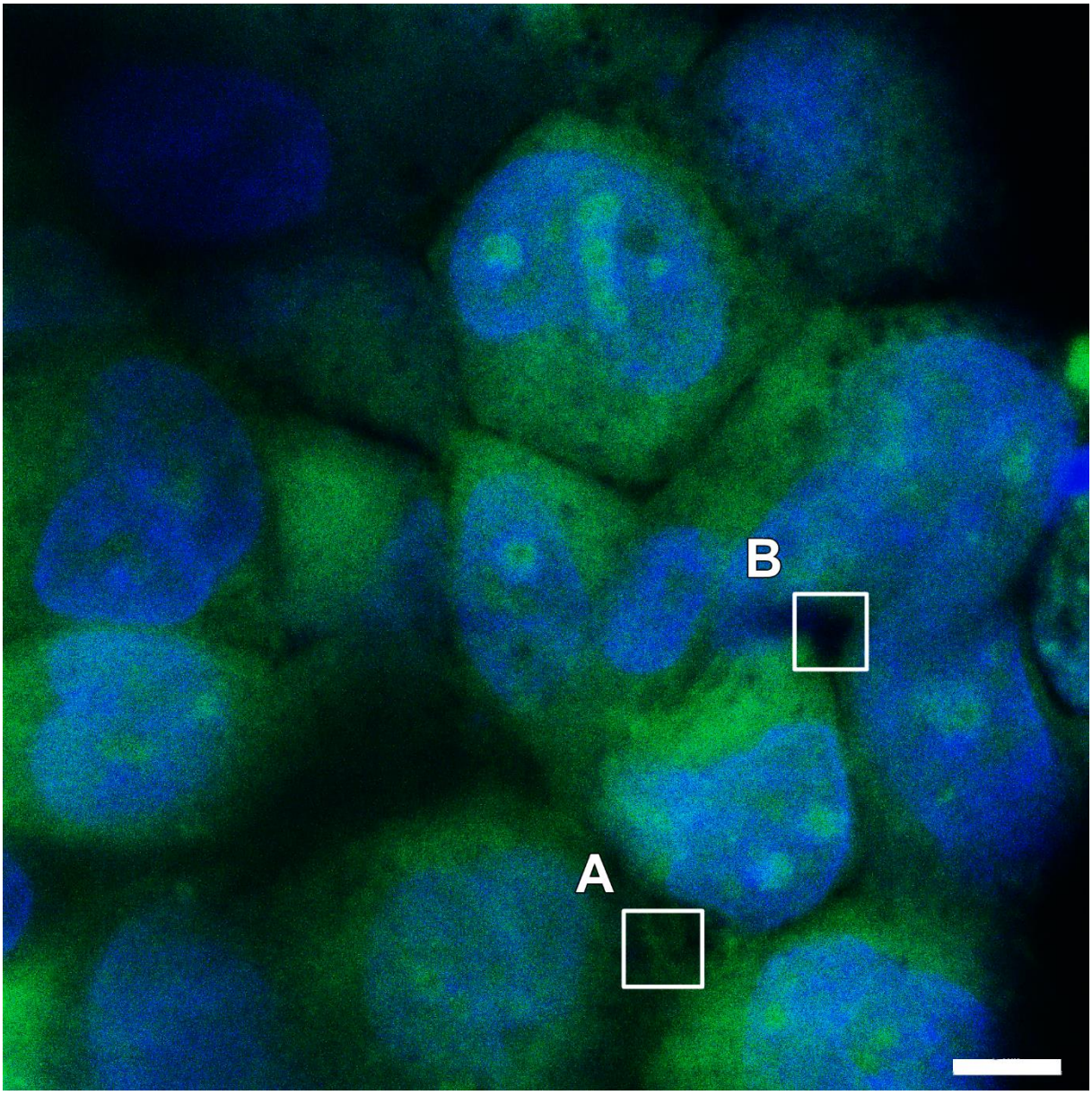

Figure S12. Confocal image of HeLa spheroid at depth of 20 μm. The ECM structure was stained with Col-F (green) and nuclei were counterstained with Hoechst 33342 (blue). Panel A represents the fibrous-rich extracellular space. In contrary, panel B depicts a large free extracellular space. The scale bar is 10 μm.

References

1. Szczepański K., Kwapiszewska K., and Hołyst R. Stability of cytoplasmic nanoviscosity during cell cycle of HeLa cells synchronized with Aphidicolin. *Scientific Reports* 2019;**9**:16486
2. Kalwarczyk T., Kwapiszewska K., Szczepański K., Soznański K., Szymański J., Michalska B., Patalas-Krawczyk P., et al. Apparent Anomalous Diffusion in the Cytoplasm of Human Cells: The Effect of Probes' Polydispersity. *The Journal of Physical Chemistry B* 2017;**121**:9831-9837
3. Stiehl O. and Weiss M. Heterogeneity of crowded cellular fluids on the meso- and nanoscale. *Soft Matter* 2016;**12**:9413-9416